

---

# A NOVEL FIRST-PRINCIPLES MODEL OF INJECTION-LOCKED OSCILLATOR PHASE NOISE.

---

arXiv PREPRINT

**Torsten Djurhuus** \*  
Goethe-University Frankfurt  
t.djurhuus@physik.uni-frankfurt.de

**Viktor Krozer**  
Goethe-University Frankfurt  
krozer@physik.uni-frankfurt.de

January 7, 2025

## ABSTRACT

The paper documents the development of a novel time-domain model of injection-locked oscillator phase-noise response. The methodology follows a first-principle approach and applies to all circuit topologies, coupling configurations, parameter dependencies *etc.* The corresponding numerical algorithm is readily integrated into all major commercial simulation software suites. The model advances current state-of-the-art pertaining to analytical modelling of this class of circuits. Using this novel analytical framework, several important new insights are revealed which, in-turn, translate into useful design rules for synthesis of injection-locked oscillator circuits with optimal noise performance.

**Keywords** phase noise, injection-locked oscillators, circuit analysis, nonlinear dynamical systems, system analysis and design

## 1 Introduction

Efficient and rigorous modelling tools for predicting phase-noise (PNOISE) response of oscillator/clock-circuits play a critical role in the design cycle of modern communication and remote-sensing systems. Given the complexity of contemporary device models, including the presence of various correlated, colored and modulated noise sources, and considering the scale of modern circuit schematics, such design work necessitates the use of an Electronic-Design-Automation (EDA) simulation environment (*e.g.* Keysight-ADS<sup>®</sup> or Cadence SpectreRF<sup>®</sup>). Relevant numerical algorithms must hence be compatible with this EDA interface. Simply stated, this requires a methodology which is formulated directly from a set of unspecified, nonlinear stochastic-differential-equations (SDE). The resulting model hence applies to any circuit regardless of topology, system dimension, parameter dependencies *etc.* Herein, this modelling strategy is referred to as a *first-principle* (FP) approach, although sometimes we may use terms such as *e.g.* unified, generalized or macro-model to describe the same concept.

The paper presents a novel time-domain (TD) FP methodology aimed at describing the PNOISE response of injection-locked oscillator (ILO) circuits; the so-called ILO phase macro-model (ILO-PMM). The model is derived as a specialization of an earlier model published by the authors [1]. The methodology is highly rigorous, being based on nonlinear stochastic integration techniques and Floquet decomposition methods. It represents a direct extension of the single oscillator phase-macro-model (PMM) developed in [4,5,9]. The ILO-PMM, however, not only extends but also replaces the standard single oscillator PMM; reverting to this representation for zero coupling. The ideas presented herein advance the current state-of-the-art (SOA) *w.r.t* modelling, analysis, synthesis and optimization of ILO noise response. The derivation of the ILO-PMM framework will be discussed in section 2.2 following a brief introduction to the underlying theory in section 2.1.

---

\*The authors are with the Institute of Physics, Goethe University of Frankfurt am Main, Max-von- Laue-Strasse 1, 60438, Frankfurt am Main. (correspondence e-mail: t.djurhuus@physik.uni-frankfurt.de).

Existing FP solutions to the problem discussed here are generally formulated as frequency-domain (FD) models involving some variation of the standard conversion-matrix (C-MATRIX) methodology [8]. These types of methods, such as *e.g.* the *pnm* algorithm which is part of the Keysight-ADS<sup>®</sup> software suite, are entirely numerical in nature with no accompanying representation for analysis purposes; herein referred to as *black-box models*. In contrast, ILO-PMM methodology produces a unique closed-form algebraic expression representing the ILO PNOISE response. This analytical interface represents an unprecedented and unparalleled feature of the ILO-PMM as no other FP description (EDA compatible model), currently published, exist with this property.

The ILO-PMM, being an analytical FP framework both extends and replaces all previous phenomenological analytical methodologies published on this topic. Such schemes are all predicated on the assumption of special ILO solution (*e.g.* the quasi-sinusoidal Kurokawa methodology [2]) or a special circuit topology (*e.g.* a block-diagram formulation). These reduced-order, empirical modelling frameworks cannot readily encompass the circuit complexities mentioned above and are obviously not compatible with the EDA interface. Nevertheless, they do, however, represent the current state-of-the-art (SOA) when it comes to mathematical/theoretical analysis of the ILO PNOISE scenario; simply because, up until this point, no fully rigorous alternatives existed. By preempting these phenomenological methodologies the ILO-PMM significantly advances the current SOA in the realm of circuit theoretical analysis. The text in sections 3, 3.1 and 3.2 discuss how the ILO-PMM can be reduced/downsized to create a equivalent FP representation of the well-established Kurokawa quasi-sinusoidal (Q-SINUS) model representation [2, 3]; referred to as the K-ILO model. Comparing the ILO-PMM and the reduced-order K-ILO model descriptions, several new insights, pertaining to the *bounds* or *range-of-application* of the Kurokawa methodology, are uncovered and discussed (see table 3.1 and lemma 3.2).

In section 4 below the capability of the proposed ILO-PMM framework is demonstrated by comparing its performance against well-established commercial numerical simulation routines. The simulations are carried out on a 0.9GHz circuit created by coupling a simple LC, negative-resistance oscillator to a CMOS, cross-coupled LC-tank unit through a unilateral buffer amplifier. The analytical ideas developed in section 3.2 are tested by comparing the outputs of the ILO-PMM and reduced-order K-ILO models, applied to the circuit described above. The work in section 4 verifies the ILO-PMM model, and the underlying theoretic ideas used to develop it. The work in both sections 3 and 4 solidifies the ILO-PMM status as the new benchmark *w.r.t.* theoretical analysis of the ILO noise scenario. The novel analytical tools introduced in this paper will prompt new insights and ideas leading to the development of design rules aimed at synthesizing ILO circuits with optimal noise performance.

## 2 Theory

The topic of discussion in this paper is the ILO-PMM, which refers to a TD, first-principles (FP) model of ILO PNOISE response. This novel result relies on theory developed by the authors in an earlier publication [1]. That paper treated the scenario of a general coupled oscillator ensemble. Below, a brief introduction to the rather complicated theoretic program, discussed in [1], is given. We then proceed show how to utilize these ideas to formulate the novel ILO-PMM model.

### 2.1 The Coupled Oscillator PMM : a Brief Review.

A novel FP (unified) model, for the prediction of the first-order stochastic response of noise-perturbed coupled oscillator ensemble, was recently published in [1] by the authors. One of the results which was achieved involved a unique closed-form expression for the PNOISE spectrum of a general ensemble. The model developed in [1] will be referred to as the coupled oscillator macro-model (COSC-PMM). The COSC-PMM framework is formulated from FP, and thus, by definition, incorporates all circuit topologies, coupling configurations and parameter dependencies in one closed-form expression. The model extends and replaces the well-established single oscillator PMM model [4, 5, 9]. The novel COSC-PMM theoretic framework was achieved by employing ideas and results from various branches of mathematics such as *e.g.* manifold-theory, differential-geometry and Floquet theory. Below, a brief review of these rather involved topics is provided. For a more detailed discussion of these issues the reader is referred to the text in [1].

Consider  $k$  free-running and asymptotically stable autonomous oscillator units coupled through some type of network; referred to herein as a  $k$ -ensemble. We assume that this network reaches a synchronized state. Let  $x \in \mathbb{R}^n$  be the  $n$ -dimensional state-space of the coupled network ( $k$ -ensemble). The synchronized PSS is then written,  $x_s(t + T_0) = x_s(t)$ , with  $T_0 > 0$  being the period of the synchronized  $k$ -ensemble. Below the  $\nu$ th harmonic of the PSS spectrum is written  $X_{s,\nu}$ . Here  $X_{s,\nu}$  is an  $n$ -dimensional vector *i.e.*  $X_{s,\nu} \in \mathbb{R}^n$ . Furthermore, the  $q$ th,  $q \in [1; n]$ , element of such a vector is written  $X_{s,\nu}^{[q]} \in \mathbb{R}$ .

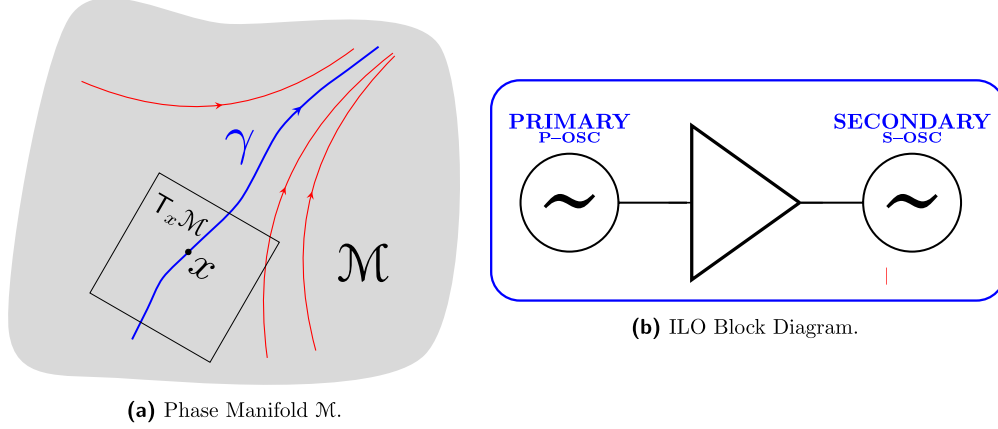


Figure 1: (a) : The limit-cycle  $\gamma$  (blue orbit) is embedded in the  $k$ -dimensional, closed, *phase-manifold*,  $\mathcal{M}$ . All orbits on, and off,  $\mathcal{M}$  approach this 1-dimensional set asymptotically with time (red orbits). The tangent-space to  $\mathcal{M}$  at a point  $x \in \mathcal{M}$ ,  $\mathbb{T}_x\mathcal{M}$ , is an affine copy of  $\mathbb{R}^k$ . (b) : Illustrating the ILO circuit configuration. The free-running primary oscillator (P-OSC) is coupled unilaterally, through some buffer amplifier to the secondary oscillator (S-OSC). Assuming a synchronized PSS is reached, the S-OSC is locked to P-OSC injected signal.

In [1] the concept of a *phase-manifold*,  $\mathcal{M}$ , is introduced. This is a closed  $k$ -dimensional space which is known to exist, for weak coupling, due to the persistence of normally hyperbolic manifolds. Furthermore, it can be shown that the ensemble limit-cycle,  $\gamma$ , is embedded in this manifold; *i.e.* it is a sub-manifold. Let  $\mathbb{T}_\gamma\mathbb{M}$  refer to the tangent-bundle, on  $\mathbb{M}$ , and along  $\gamma$  where the concept of a tangent-bundle simply refers to the disjoint union of tangent-spaces (affine copies of vector-space  $\mathbb{R}^k$ ) along  $\gamma$ ; *i.e.*  $\mathbb{T}_\gamma\mathbb{M} = \{\mathbb{T}_x\mathbb{M}\}_{x \in \gamma}$ . As detailed in [1], there exists exactly  $k$  Floquet vectors  $\{u_i(t)\}_{i=1}^k$  which span the bundle  $\mathbb{T}_\gamma\mathbb{M}$ . These  $k$  modes, also known as the *phase-modes*, govern the PNOISE response of the  $k$ -ensemble. The scenario discussed here is illustrated in fig. 1.(a).

The setup described above and in fig. 1.(a), assures the existence of  $k$  unique Floquet phase-modes  $\{u_i(t)\}_{i=1}^k$ . It is then possible to calculate the PNOISE response which is the response spanned by these operators. Following some rather lengthy and involved calculations, an expression for the PNOISE spectral density of a  $k$ -ensemble was derived in [1, sec. 6] which we repeat here

$$\mathfrak{L}^{(\nu)}(\omega_m^{(\nu)}) = \frac{(1 - a^{(\nu)})(\omega_0^2 c) - 2b^{(\nu)}\omega_m}{(0.5\omega_0^2 c)^2 + (\omega_m^{(\nu)})^2} + \sum_{\rho} \sum_{l=2}^k \frac{\Upsilon_{l\rho}^{(\nu)} [2|\mu_{l,r}| + (\omega_0^2 \rho^2 c)] + 2\Delta_{l\rho}^{(\nu)} [\omega_m^{(\nu)} + \mu_{l,i}]}{(|\mu_{l,r}| + (0.5\omega_0^2 \rho^2 c))^2 + (\omega_m^{(\nu)} + \mu_{l,i})^2} \quad (1)$$

with  $\omega_0 = 2\pi/T_0$  being the operating frequency of the synchronized ensemble, superscript, index  $\nu$  refers carrier harmonic around which the PNOISE response is calculated,  $\mu_s = \mu_{s,r} + j\mu_{s,i} \in \mathbb{C}$ , is the  $s$ th characteristic Floquet exponent (real/imaginary parts) and  $\omega_m^{(\nu)} = \omega - \nu\omega_0$  is the  $\nu$ th harmonic offset frequency. The real parameter,  $c \in \mathbb{R}_+$ , is known as the *phase-diffusion* constant [4–6, 9]. All sums in eq. (1) w/o bounds operate in the interval  $(-\infty, \infty)$ . The operators  $a^{(\nu)}$ ,  $b^{(\nu)}$ ,  $\Upsilon_{l\rho}^{(\nu)}$ ,  $\Delta_{l\rho}^{(\nu)}$  introduced in eq. (1) are defined through

$$a^{(\nu)} + jb^{(\nu)} = [\Omega^{(\nu)}]_{q,q} / \|X_{s,\nu}^{[q]}\|^2 \quad (2)$$

$$\Upsilon_{l\rho}^{(\nu)} + j\Delta_{l\rho}^{(\nu)} = [\Theta_{l\rho}^{(\nu)}]_{q,q} / \|X_{s,\nu}^{[q]}\|^2 \quad (3)$$

where index  $q$  refers to the index of the *observation-node* *i.e.* the node where PNOISE is measured,  $[S]_{x,y}$  denotes to the element at row  $x$  and column  $y$  of matrix  $S$  and  $X_{s,\nu}^{[q]}$  refers to the  $q$  element of the PSS  $\nu$ th harmonic vector (see discussion above). The two complex tensor operators  $\Omega$  and  $\Theta_{l\rho} \in \mathbb{C}^{n \times n}$  have the form (see [1, appendix B] for details)

$$\Omega^{(\nu)} = \sum_{m=2}^k \sum_p \frac{U_{1,\nu} \Lambda_{1,0}^\top \Lambda_{m,\nu-p}^* U_{m,p}^\dagger}{j\omega_0(p-\nu) - \mu_m^*} \quad (4)$$

$$\Theta_{l\rho}^{(\nu)} = \frac{U_{1,\rho} \Lambda_{1,0}^\top \Lambda_{l,\rho-\nu}^* U_{l,\nu}^\dagger}{j\omega_0(\nu-\rho) - \mu_l^* - \mu_1} + \frac{\sum_{i=2}^k \sum_p U_{i,p} \Lambda_{l,\rho-p}^\top \Lambda_{l,\rho-\nu}^* U_{l,\nu}^\dagger}{j\omega_0(\nu-p) - \mu_m^* - \mu_i} \quad (5)$$

with  $U_{i,j} \in \mathbb{C}^n$  being the  $j$ th harmonic of the  $i$ th Floquet phase-mode vector  $u_i(t) : \mathbb{R} \rightarrow \mathbb{C}^n$  and  $\Lambda_{i,j} \in \mathbb{C}^n$  is the  $j$ th harmonic of the  $i$ th Floquet phase-mode lambda-vector  $\lambda_i(t) : \mathbb{R} \rightarrow \mathbb{C}^n$  where  $\lambda_i(t) = v_i^\top(t)B(x_s(t))$ , with  $v_i(t) : \mathbb{R} \rightarrow \mathbb{C}^n$  being the  $i$ th Floquet phase-mode dual-vector. Finally,  $B(x_s(t)) : \mathbb{R} \rightarrow \mathbb{R}^{n \times p}$  is the noise modulation matrix, see *e.g.* [1,4,5,9], which describes how  $p$  white-noise sources are injected into the  $n$ -dimensional state-space and the manner in which the sources are modulated by the PSS,  $x_s(t)$ .

## 2.2 An Injection Locked Oscillator PMM : the ILO-PMM.

The ILO configuration is illustrated in fig. 1.(b). As can be seen, the coupled ensemble involves 2 oscillator units, with the secondary oscillator (S-OSC) coupled to the primary oscillator (P-OSC) through some unilateral buffer/amplifier circuit. Since we are considering 2 coupled units it follows from the discussion in section 2.1, that there will exist two real Floquet phase-modes ( $\mu_1 = 0, \mu_2 < 0$ ) governing the synchronized ILO PNOISE response. Considering the PNOISE spectrum around the 1st PSS harmonic spectrum ( $\nu = 1$ ), and given the setup with 2 phase-modes ( $k = 2$ ), the general expression in eq. (1) specializes to the following model for an ILO circuit

$$\mathfrak{L}_{\text{ILO}}(\omega_m) = \frac{(1-\alpha)(\omega_0^2 c) - 2\beta\omega_m}{(0.5\omega_0^2 c)^2 + \omega_m^2} + \sum_p \frac{\Delta_\rho [2|\mu_2| + (\omega_0^2 \rho^2 c)] + 2\Gamma_\rho \omega_m}{(|\mu_2| + (0.5\omega_0^2 \rho^2 c))^2 + \omega_m^2} \quad (6)$$

where the notation,  $\mu_2 = \mu_{2,r}$ , was used since we know that the second phase mode is real and

$$\alpha + j\beta = [\Psi]_{q,q} / \|X_{s,1}^{[q]}\|^2 \quad (7)$$

$$\Delta_\rho + j\Gamma_\rho = [\Phi_\rho]_{q,q} / \|X_{s,1}^{[q]}\|^2 \quad (8)$$

Here  $q$ , again, denotes the observation node (see discussion in section 2.1) and the various complex tensor operators are given through

$$\Psi = \sum_p \frac{U_{1,1} \Lambda_{1,0}^\top \Lambda_{2,1-p}^* U_{2,p}^\dagger}{j\omega_0(p-1) - \mu_2} \quad (9)$$

$$\Phi_\rho = \frac{U_{1,\rho} \Lambda_{1,0}^\top \Lambda_{2,\rho-1}^* U_{2,1}^\dagger}{j\omega_0(1-\rho) - \mu_2} + \frac{\sum_p U_{2,p} \Lambda_{2,\rho-p}^\top \Lambda_{2,\rho-1}^* U_{2,1}^\dagger}{j\omega_0(1-p) - 2\mu_2} \quad (10)$$

The result in eqs. (6) to (10) describes the ILO-PMM. This model represents the first ever, at-least to the author's knowledge, rigorous TD FP (non-phenomenological/empirical) representation of ILO PNOISE response. Established FP methodologies, such as *e.g.* the C-MATRIX class of FD algorithms used in *e.g.* the *pnm* routine implemented in the Keysight-ADS<sup>®</sup> EDA suite, are exclusively numerical in nature *i.e.* *black-box routines* (see discussion in introduction). The ILO-PMM advances the current SOA by providing an explicit closed-form expression for the ILO PNOISE spectrum. The rigorous ILO-PMM modelling framework both advances and repairs the flawed linearized FD FP schemes (*e.g.* the C-MATRIX methodology), involving, among other things, artificial singularities in the PNOISE spectrum [5], by calculating the response through direct stochastic integration of the raw nonlinear circuit SDE's [1]. The addition of the new analytical tool-set, discussed above, will lead to the invention of new design rules for synthesis of circuits with optimal noise performance.

## 3 Comparing the ILO-PMM to Established Analytical Models.

The ILO-PMM framework, eqs. (6) to (10), represents the only example of a FP (*i.e.* non-phenomenological/empirical) analytical model of ILO noise response. Given this fact, the following question is relevant : why does the ILO-PMM

not resemble the earlier, well-established analytical model representations? The disconnect becomes obvious when comparing eq. (6) the established standard form of the ILO PNOISE spectral characteristic which can be written [2, 3, 14–16]

$$\widehat{\mathcal{L}}_{\text{ILO}}(\omega_m) = \frac{\Omega_{3\text{dB}}^2 \mathcal{L}_{\text{P}}(\omega_m) + N_{\text{S}}}{\omega_m^2 + \Omega_{3\text{dB}}^2} \quad (11)$$

where  $\Omega_{3\text{dB}}$  is the pole of the ILO spectrum  $\mathcal{L}_{\text{P}}(\omega_m) : \mathbb{R} \rightarrow \mathbb{R}$  is the PNOISE spectrum of the free-running P-OSC and  $N_{\text{S}} \in \mathbb{R}$  is some scalar representing noise-contribution from the S-OSC circuit (see fig. 1.(b)). The standard-form characteristic in eq. (11) is generally reached using less rigorous methods (see discussion below), however, this does not overturn the fact such schemes have been highly successful in predicting the noise response of a large class of important circuits. It is therefore essential to be able to relate and connect the ILO-PMM, developed herein, to these earlier well-established results. Below, this issue is confronted within the context of the single most successful and influential model ever published on ILO noise response : the Kurokawa model [2].

### 3.1 The Kurokawa Methodology.

In 1968 by Kaneyuki Kurokawa developed a novel methodology for predicting the noise-response of near-sinusoidal (high-Q) ILO circuits perturbed by weak noise sources. His approach centered around a *quasi-sinusoidal* assumption for the full noisy ILO solution and a restriction to a planar representation for the oscillator units (*i.e.* 2-D oscillators). The term *quasi-sinusoidal* (Q-SINUS) implies that the PSS can be approximated as purely sinusoidal (higher harmonics are discarded) with a slow-moving phase/amplitude envelope<sup>2</sup> induced by the weak noise source drive. The novel modelling strategy, developed in the seminal paper [2] (see footnote 2 for a brief review), has since proved highly successful in developing useful models for all kinds of oscillator configurations (coupled and singles) driven by weak noise [3, 10–12, 14–16]. The Kurokawa methodology represents an example of the phenomenological/empirical modelling approach discussed above. It is given this label since it is predicated on a specific type of oscillator PSS (sinusoidal), a specific type of solution (*i.e.* Q-SINUS), and furthermore is restricted to 2-D oscillator units. Below, the Q-SINUS modelling approach is briefly introduced, and it is then shown how to connect this important methodology to the novel FP representation proposed herein.

#### 3.1.1 Rediscovering the Kurokawa Model : Creating Reduced-Order Equivalent Model.

Both the ILO-PMM framework, which applies to all possible ILO circuits and solutions (see discussion in section 2.2), and the Kurokawa model claim to correctly predict the PNOISE response of an ILO circuit generating a Q-SINUS solution. Given this fact, it must then be possible to somehow connect these two very different methodologies. Indeed, as will be shown, it is possible to construct reduced-order model description, the K-ILO model, from the ILO-PMM framework which constitutes an equivalent FP representation of the original phenomenological Kurokawa model. The purpose of performing this operation is two-fold as will now be discussed.

1. By producing this reduced-order K-ILO model we are effectively proving that the ILO-PMM supersedes and encompasses the Kurokawa Q-SINUS methodology. This result is not limited to the specific Kurokawa model but extends to most, if not all, non-rigorous/approximative modelling strategies. This must be so since the ILO-PMM represents a FP (non-phenomenological) analytical model which is applicable to all possible circuits and solutions. Hence, any such non-rigorous, phenomenological and/or empirical modelling attempt must be represented within the ILO-PMM framework as a reduced-order sub-model. The ILO-PMM hence both extends and replaces all these previously published non-rigorous analytical models. This result advances the SOA in the field of ILO noise analysis. It is of fundamental importance with far-reaching implications for future research.
2. Developing the FP reduced-order, equivalent Kurokawa model gives unique insights into which components of the original representation are expunged or neglected in-order to reach this downsized version. The analytical work allows us to understand and quantify the *bounds* of these phenomenological strategies. It establishes a range-of-application (see table 3.1 and lemma 3.2 below) for the Kurokawa (Q-SINUS) class of models.

---

<sup>2</sup>The Kurokawa ILO PSS is written  $x_s(t) = \Re\{A_0 \exp(j\omega_0 t + \phi_0)\}$ , where  $A_0, \phi_0 \in \mathbb{R}$  are the steady-state amplitude and phase offset parameters. The full noise-perturbed solution is then written  $x(t) = x_s(t) + \delta x(t) = \Re\{A(t) \exp(j\phi(t))\}$ , where  $\delta x(t) : \mathbb{R} \rightarrow \mathbb{R}^2$  is the slow-moving envelope which can be written in-terms of the amplitude and phase envelopes  $\delta_{A/\phi}(t)$  *i.e.*  $A(t) = A_0 + \delta_A(t)$ , and  $\phi(t) = \omega_0 t + \phi_0 + \delta_\phi(t)$ . Using this notation a complex envelope equations can be formulated. Using averaging methods, real differential equations for the envelopes,  $\delta_{A/\phi}(t)$ , are derived. Finally, Fourier transforming these expressions the PNOISE spectrum can be calculated which takes the form shown in eq. (11).

Outside this range, this type of model breaks down *i.e.* is no longer able to correctly predict the response. This is an important result which furthers our understanding of ILO noise modelling and analysis with many potential applications for practical circuit design.

The analysis starts with the following result.

**lemma 3.1.** *Assuming Q-SINUS operation, a reduced-order representation of the ILO-PMM, referred to as the K-ILO model, can be calculated. This model is an equivalent version of the original Kurokawa result [2]. The PNOISE spectrum,  $\mathfrak{L}_{K-ILO}(\omega_m)$ , calculated using this reduced-order model has the form*

$$\mathfrak{L}_{K-ILO}(\omega_m) = \frac{\Delta_0^{(K)} + |\mu_2|^2 \mathfrak{L}_P(\omega_m)}{|\mu_2|^2 + \omega_m^2} \quad (12)$$

with  $\Delta_0^{(K)} \in \mathbb{R}$  being a real scalar defined through

$$\Delta_0^{(K)} = 2 [ U_{2,1} \Re \{ \Lambda_{2,1}^\top \Lambda_{2,1}^* \} U_{2,1}^\dagger ]_{q,q} / \| X_{s,1}^{[q]} \|^2 + 5\omega_0^2 c \quad (13)$$

where all parameters and notation is explained in section 2.1 (see text accompanying eqs. (4) and (5)) and  $\mathfrak{L}_P(\omega_m) : \mathbb{R} \rightarrow \mathbb{R}$  refers to the PNOISE spectrum of the free-running P-OSC circuit (see fig. 1.(b)).

*Proof.* see appendix A □

Comparing eq. (12) with the standard-form expression in eq. (11) yields  $|\mu_2| = \Omega_{3dB}$  and  $\Delta_0^{(K)} = N_s$ .

### 3.2 Comparing the ILO-PMM to the Reduced-Order K-ILO Model.

The K-ILO model, derived above in lemma 3.1, is a *reduced-order* version of the complete FP ILO-PMM scheme derived in section 2.2. By definition, this implies that the ILO-PMM must contain additional information not available in this Kurokawa equivalent model representation. Below we set out to quantify these ideas. The purpose and motivation for this work was discussed above. Comparing the ILO-PMM and K-ILO models, defined in eqs. (6) to (10) and eqs. (12) and (13), several interesting differences are observed. Three of these are listed in table 3.1 and the main conclusions from this discussion are summarized in lemma 3.2 below.

**lemma 3.2** (Kurokawa Model Range-of-Application). *The Kurokawa Q-SINUS methodology, as described in [2], will fail to correctly predict the ILO PNOISE spectrum if the circuit PSS induces, **1**) :  $\Lambda_{1,0} \neq 0$ , **2**) :  $\Lambda_{2,i} \neq 0$  for  $i \neq \pm 1$ , **3**) :  $|\mu_2| \sim \omega_0^2 c$  (strong P-OSC noise drive).*

*Proof.* follows directly from the discussion in table 3.1 and the fact that the Kurokawa and K-ILO model representations are equivalents. □

## 4 Numerical Experiments

Consider the ILO circuit created by coupling the two oscillator units, shown in fig. 2, according to the diagram in fig. 1.(b). Here the LC oscillator, OSC1, is connected unilaterally, through a buffer amplifier, to the cross-coupled CMOS unit, OSC2. Following the schematic in fig. 1.(b), OSC1, the P-OSC, is free-running while OSC2, the S-OSC, assuming a synchronized PSS is reached, will be locked to the injected signal. The circuit described here oscillates at a frequency around  $f_0 = 1/T_0 = 0.9\text{GHz}$ . Herein, this circuit will be used in a series of simulation trials aimed at investigating and verifying the novel ILO-PMM framework, which was developed above in section 2.2. A study is conducted, comparing the spectrum, calculated using the ILO-PMM framework, with the results produced by the *pnmx* numerical routine; a module contained in the commercial Keysight-ADS<sup>®</sup> EDA suite. Specific attention is furthermore paid to the points raised in table 3.1 and lemma 3.2. The purpose of this exercise is to explore the operational bounds of the phenomenological Kurokawa methodology, represented herein by the reduced-order K-ILO equivalent model developed in lemma 3.1.

Figure 3.(a) shows the ILO PSS for a select number of circuit nodes of oscillator units shown in fig. 2. Here, the oscillator units are coupled linearly with  $g_{c1} = 35.0\mu\text{A/V}$  (see fig. 2 caption). From this figure it follows that node  $v_{cg}$  contains significant higher harmonic content (*i.e.* 2nd, 4th *etc.*) as this is a common-ground node. The PSS at this node does therefore not conform to the near-sinusoidal PSS description on which the K-ILO reduced-order model

1. The development of the K-ILO model involved the assumption  $\Lambda_{1,0} = 0$  (*i.e.* zero DC component of  $\lambda_1$ , see section 2.1). For circuits with  $\Lambda_{1,0} \neq 0$  the K-ILO spectrum might differ significantly from the correct FP ILO-PMM solution. The exact issues causing,  $\Lambda_{1,0} \neq 0$ , for a given circuit are not always entirely understood or easily described. This is especially true for higher dimensional ( $n > 2$ ) systems. It is in many cases a consequence of strongly non-linear circuit nodes which induce DC components in the corresponding dual Floquet vector,  $v_1(t)$ , (see text accompanying eqs. (12) and (13)). Furthermore, a non-constant noise modulation matrix,  $B(x_s(t))$ , often induces the aforementioned result due mixing products landing at DC.
2. The K-ILO model further assumes that the DC and higher-order terms of  $\lambda_2$  be zero *i.e.*  $\Lambda_{2,i} = 0$ , for  $i \neq \pm 1$ . Loosely speaking, this scenario could be induced by simply by the presence of non-sinusoidal nodes in the circuit PSS vector. In other words, non-sinusoidal PSS nodes could, to a certain extent at-least, induce non-sinusoidal nodes in  $\lambda_2$ . This relation, described here, is only based on empirical observation and is in no way to be considered a scientific law. It is not generally not known how the harmonic content of a linear-response operator, like  $\lambda_2$ , is connected to the underlying PSS, especially not for higher dimensional circuits. Nevertheless, in section 4 below, an example is discussed where a noise-source, injected into a common-ground node (non-sinusoidal PSS node) of a cross-coupled CMOS circuit, results in a non-sinusoidal  $\lambda_2$  node.
3. The original ILO-PMM model describes the spectrum as an infinite sum of Lorentzian spectra (see eqs. (6) to (10)) whereas the standard characteristic only involved the sum of two such spectra (see eqs. (11) to (13)). As was discussed in appendix A, for a strong noise drive we have  $|\mu_2| \sim \omega_0^2 c$  (same order of magnitude) and the poles of the Lorentzians in the sum separate and each term in eq. (6) must be included separately. Here, the reduced-order K-ILO model will, once again, diverge from the correct response. For weak noise drive, which is the case consider herein,  $|\mu_2| \gg \omega_0^2 c$  and the poles are more-or-less constant for all indices of interest (for larger indices the terms in eq. (6) will approach zero with the nominator of the fractions) and we regain the single-pole characteristic predicted in eq. (12).

Table 3.1: Comparing the ILO-PMM, eqs. (6) to (10), to the reduced-order K-ILO model, eqs. (12) and (13). Note that since the K-ILO is an equivalent representation of the original Kurokawa model [2] all conclusions apply equally to this methodology (see lemma 3.2).

is built (see discussion in appendix A). In fig. 3.(b), the ILO-PMM PNOISE spectral-density, derived from eq. (6), is plotted for two parameters sets (see figure caption), together with corresponding curves produced by the *pnmx* numerical routine. Inspecting fig. 3, the solutions of these two, qualitatively very different, numerical algorithms (ILO-PMM/*pnmx*) seem to overlap for the most of the frequency range, further verifying the novel FP model proposed herein.

#### 4.1 Exploring Point #1 of Table 3.1.

The circuit in fig. 2 does not involve modulated noise meaning that the noise-modulation matrix  $B \in \mathbb{R}^{n \times p}$  is constant. The  $p$  columns of,  $B$ , each correspond to one of the resistors or external current noise sources in this circuit. Let  $j_{w,n} \in [1, p]$  be the noise-indices corresponding to the two external noise sources  $w(t), n(t) : \mathbb{R} \rightarrow \mathbb{R}$  seen in fig. 2. These two noise These two sources dominate the noise response, described in-terms of the lambda functions  $\lambda_i(t) = v_i^T(t)B : \mathbb{R} \rightarrow \mathbb{R}^p$ ,  $i = 1, 2$  (see discussion in sections 2.1 and 2.2). Let  $\lambda_{i,j}(t)$  denote the  $j$ th component of this  $p$ -dimensional vector, then fig. 4.(a) plots  $\lambda_{1,j_w}(t)$ ,  $\lambda_{2,j_w}(t)$ ,  $\lambda_{2,j_n}(t)$ . Note that the S-OSC (OSC2) noise-source,  $n(t)$ , does not contribute to  $\lambda_1$ . From fig. 4.(a) it follows that the dominant noise node component of  $\lambda_1$ , *i.e.*  $\lambda_{1,j_w}(t)$ , has zero DC,  $\Lambda_{1,0} = 0$ . Following the discussion in point #1 of table 3.1, this outcome was expected as the OSC1 circuit shown in fig. 2 sinusoidal in nature and hence conform to the Q-SINUS (Kurokawa) representation. The requirement,  $\Lambda_{1,0} = 0$ , upon which the reduced-order Q-SINUS K-ILO model (see sections 3 and 3.2) was conditioned, is hence seen to hold for the circuit in fig. 2. At this point it would seem that the ILO circuit considered here complies with the Q-SINUS Kurokawa methodology. This would then suggest that the reduced-order K-ILO equivalent model (see lemma 3.1) could substitute for the full FP ILO-PMM description in eqs. (6) to (10) as a reasonable approximation for th circuit discussed here. However, as will be shown below, this assumption is false.

#### 4.2 Exploring Point #2 of Table 3.1 - the Breakdown of the Kurokawa Approach.

Figure 4.(a) plots  $\lambda_{2,j_w}(t)$  and  $\lambda_{2,j_n}(t)$ , representing contribution, due to noise sources  $w(t), n(t)$ , to the vector  $\lambda_2$  (see section 3.1). Here  $\lambda_{2,j_w}(t)$  is again is almost a pure sinusoidal. However, it is clear that  $\lambda_{2,j_n}(t)$  does not fit this description. This should come as no surprise since  $n(t)$  is injected into the common-ground node of the cross-

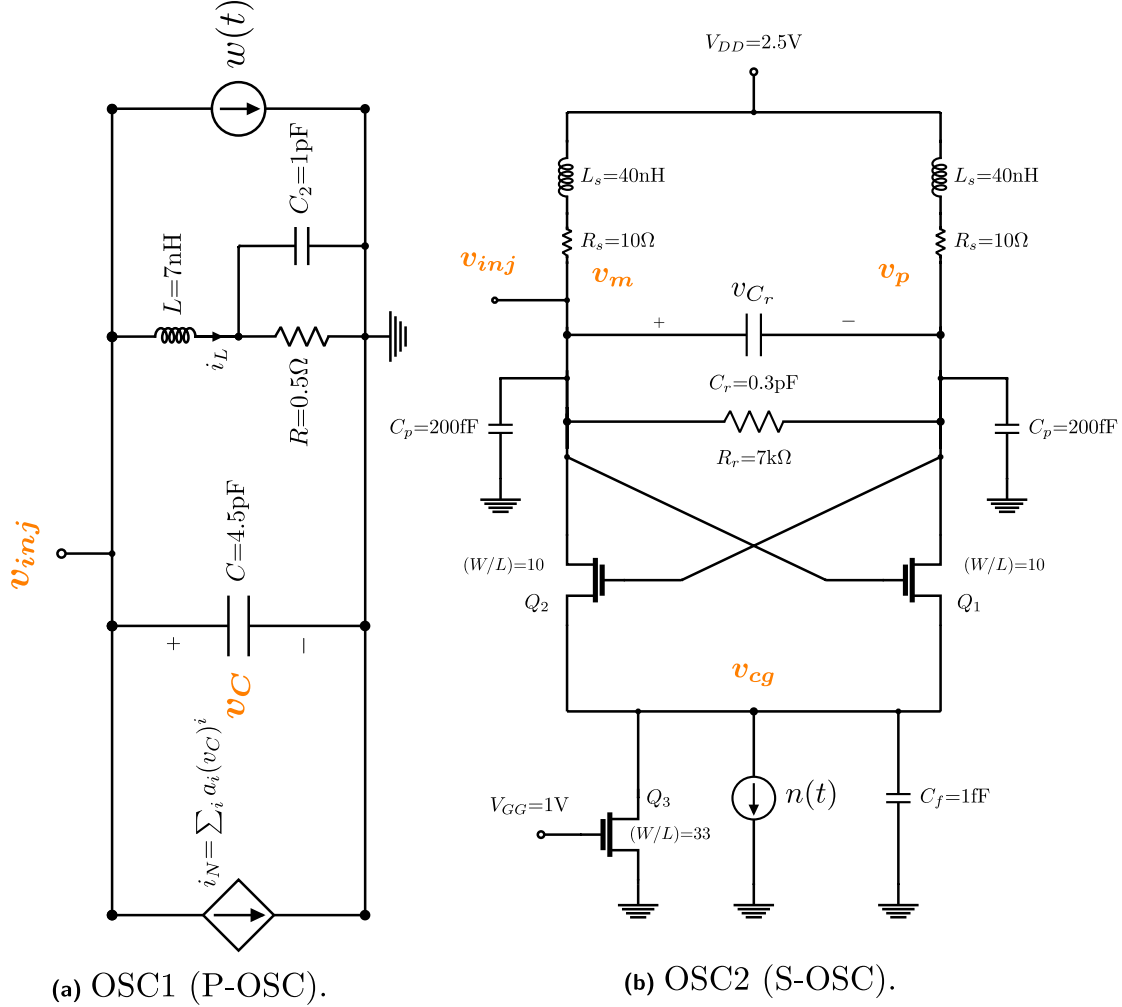


Figure 2: The figure shows the two oscillator units which are coupled, as shown in fig. 1.(b), to produce the ILO circuit discussed here. The unilateral buffer amplifier (see fig. 1.(b)), which connects to two circuits through the  $v_{inj}$  ports, has a 4th order polynomial in-out characteristic  $v_{out} = \sum_{k=0}^3 g_{ck}(v_{in})^k$ . Component values are fixed to values shown unless otherwise stated. (a) : OSC1 (P-OSC) is a simple LC negative-resistance oscillator. Free-running oscillation frequency  $f_0 = 900.9\text{MHz}$ , corresponding to a period of  $T_0 = 1.11\text{ns}$ . VCCS (negative resistor) parameters :  $a_1 = -1.0\text{mS}$ ,  $a_3 = 100\mu\text{A}/\text{V}^3$  and  $a_i = 0$  for  $i \neq 1, 3$ . The white-noise current source,  $w(t)$ , has the rms current strength  $i_{w,rms} = 1\text{pA}/\sqrt{\text{Hz}}$ . (b) : OSC2 (S-OSC) is a CMOS cross-coupled LC-tank circuit. Free-running oscillation frequency  $f_0 = 892.86\text{MHz}$ , corresponding to a period of  $T_0 = 1.12\text{ns}$ . The CMOS devices are considered noiseless. The rms current of white-noise source,  $n(t)$ , is given as  $i_{n,rms} = 70.7\text{pA}/\sqrt{\text{Hz}}$ . CMOS model (all transistors) :  $V_{th0} = 0.5\text{V}$ ,  $\lambda = 0.05\text{V}^{-1}$ ,  $k_p = 120\mu\text{A}/\text{V}^2$  which is also the model used in [17]. The CMOS channel width-to-length ratios are listed next to the respective components.

coupled CMOS oscillator OSC2 shown in fig. 2.(b). As noted above (see fig. 3.(a)), the PSS at this node does not fit the near-sinusoidal PSS requirement. Therefore, one should also not expect (loosely speaking) the lambda-vector components to conform either (see # 2 of table 3.1). The observation implies that the reduced-order K-ILO equivalent developed in section 3.1.1, should fail to capture the correct response. This can be observed in fig. 4.(b) which plots the PNOISE spectral density of the circuit in fig. 2 for the linear coupling  $g_{c1} = 35.0\mu\text{A}/\text{V}$ . The figure shows the spectrum calculated using the both the ILO-PMM (eqs. (6) to (10)) and K-ILO (eqs. (12) and (13)) methods as well as the numerical *pnm* routine. From this figure it is clear that the K-ILO model fails to capture the spectrum especially for higher offsets which, which is due to the contribution of higher-harmonic content of  $\lambda_{2,j_n}(t)$  shown in fig. 4.(a). To further prove this point, the intensity of the common-ground noise source  $n(t)$  is now decreased from  $70.0\text{pA}/\sqrt{\text{Hz}}$



to  $70.7\text{fA}/\sqrt{\text{Hz}}$ . Naturally, this will diminish the effect of the contribution  $\lambda_{2,j_n}(t)$  shown in fig. 4.(a). Instead, the contribution due to P-OSC source,  $w(t)$ , as represented by the component function,  $\lambda_{2,j_w}(t)$ , will dominate the second mode response. From fig. 4.(a), this contribution is highly sinusoidal which in-turn implies that modified circuit adheres to the Kurokawa model requirements (see appendix A). Consequently, one should expect the reduced-order K-ILO model, developed in section 3.1.1, to capture correct response of the modified circuit. Figure 5, once again, plots the spectrum of the circuit in fig. 2 (see fig. 4 caption) but this time with  $w(t) = 70.7\text{fA}/\sqrt{\text{Hz}}$ . As predicted, the simple reduced-order K-ILO model now captures the correct PNOISE response. Finally, from lemma 3.2, all results and conclusions discussed here, related to the reduced-order K-ILO model developed in lemma 3.1, extend directly to the entire class of ILO PNOISE models built using the Q-SINUS methodology including the original well-established and highly referenced original representation in [2].

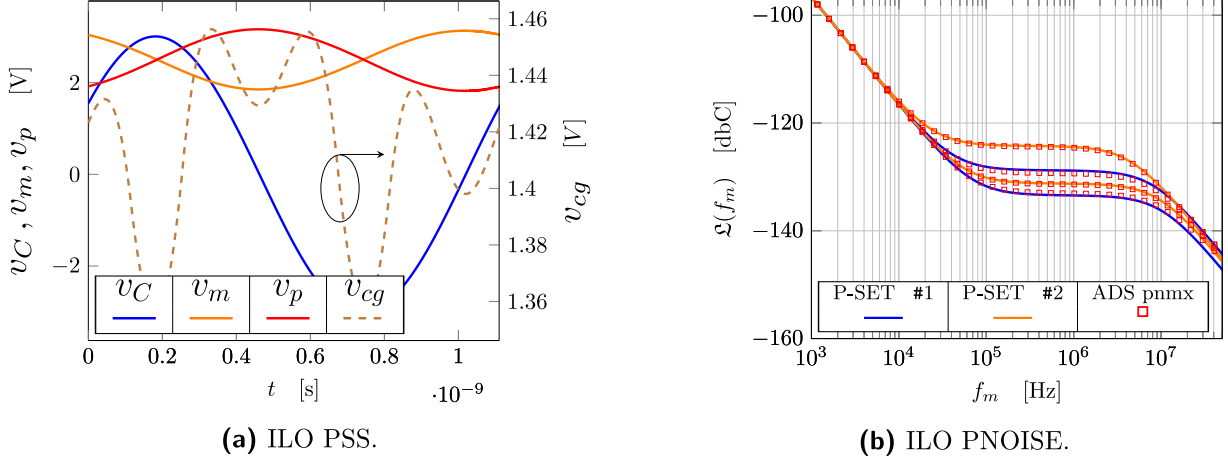


Figure 3: (a) : PSS solution of the ILO circuit shown in fig. 2. (b) : phase-noise spectral densities for the ILO circuit in fig. 2. The figure shows the PNOISE spectrum for the ILO circuit calculated using the novel ILO-PMM model developed herein along with the corresponding output of the *pnmX* routine, part of the Keysight-ADS<sup>®</sup> suite. The simulations are run for two parameter sets, PSET1 : ( $C_r = 0.3035\text{pF}, 0.295\text{pF}, g_{c1} = 35\mu\text{A/V}$ ) and PSET2 : ( $g_{c1} = 40\mu\text{A/V}, 60\mu\text{A/V}$ ) with all other component values and circuit parameters fixed as listed in fig. 2.

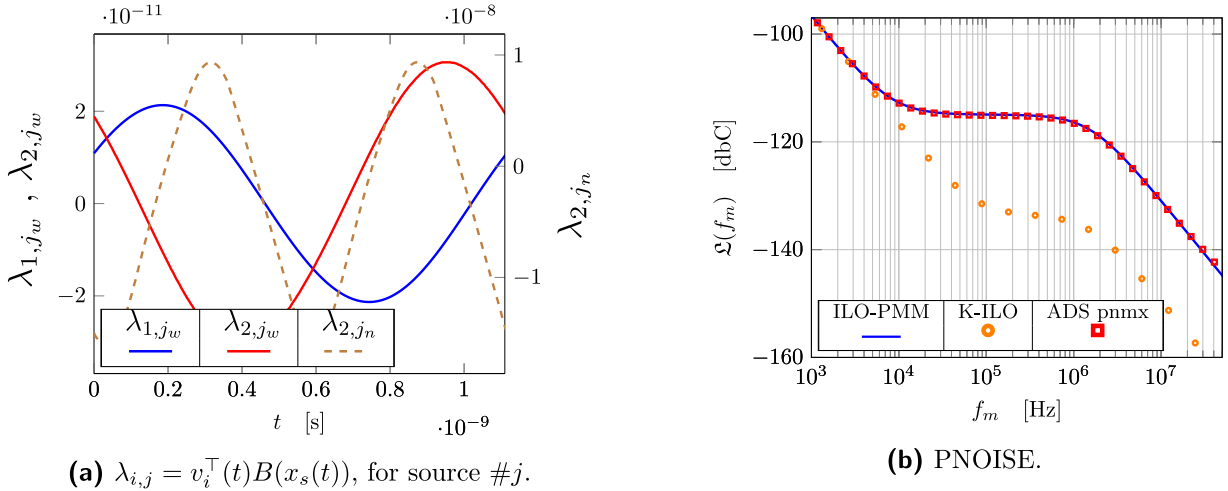


Figure 4: (a) : figure shows the components of  $\lambda_i(t) = v_i^T(t)B$ ,  $i = 1, 2$ , corresponding to Floquet modes  $\mu_1 = 0, \mu_2 < 0.0$ , and representing the contributions due to noise sources  $n(t), w(t) : \mathbb{R} \rightarrow \mathbb{R}$  (see fig. 2) which dominate the response. (b) : the PNOISE spectrum calculated using ILO-PMM, K-ILO model and the *pnmX* routine. Due to the DC and even harmonic components of the contribution  $\lambda_{2,j_n}(t)$  (see figure (a)) the reduced-order K-ILO model fails to predict the correct spectrum for higher offset frequencies.

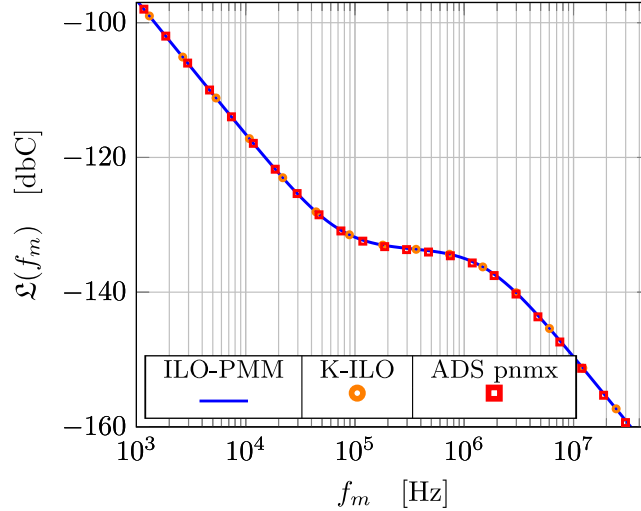


Figure 5: PNOISE spectrum of the modified circuit (see discussion in text). The spectrum is calculated using the ILO-PMM, K-ILO model and *pnm* method. The modified circuit generates a solution which conforms to Q-SINUS/Kurokawa methodology and the reduced-order K-ILO equivalent model is hence able to correctly predict the ILO PNOISE response. This should be contrasted with the result reported in fig. 4.(b) above.

## 5 Conclusion

We document the development of a novel time-domain model of injection-locked oscillator phase-noise response; the so-called ILO-PMM. The methodology is based on a rigorous first-principles approach and, as such, is applicable to all circuit topologies, system dimension, parameter dependencies *etc.* The companion numerical algorithm is compatible with all major commercial circuit simulation programs. We explore the analysis of circuits from a macro-model perspective. It is shown that the ILO-PMM, developed herein, extends and replaces the standard models currently found in the literature on this topic. The work discussed herein advances the current state-of-the-art *w.r.t.* both numerical and theoretical modelling and analysis of injection-locked oscillator noise response. Several new insights are uncovered with the potential for important practical design applications. The analytical innovations and ideas discussed herein will serve as inspiration for future publications currently being written.

## Acknowledgment

The authors gratefully acknowledge partial financial support by German Research Foundation (DFG) (grant no. KR1016/17-1).

## A Proof of lemma 3.1.

Below we consider the concept of a *near-sinusoidal* (N-SINUS) vector-function,  $y(t) : \mathbb{R} \rightarrow \mathbb{R}^n$

$$y(t) = \alpha + x(t) + \mathcal{O}(\epsilon)s(t) \quad (14)$$

where  $\alpha \in \mathbb{R}^n$  is the DC component of the signal,  $x(t) : \mathbb{R} \rightarrow \mathbb{R}^n$  is a pure sinusoidal vector-function (*i.e.* no higher harmonics),  $s(t) : \mathbb{R} \rightarrow \mathbb{R}^n$  is a scaled vector function  $|s(t)| \leq 1$  for all  $t$ , containing all higher harmonics and  $|\epsilon| \ll 1$  a small parameter. The definition in eq. (14) describes a signal which is *almost* sinusoidal which is the case for the PSS in the Kurokawa Q-SINUS methodology (see [2, 3]).

For an autonomous oscillating system, such as a locked ILO circuit, the special Floquet mode  $\mu_1 = 0$ , is known to exist [4, 5, 9]. Furthermore, it is well established [4, 5, 9], that the Floquet vector  $u_1(t)$  is a scaled copy of  $\dot{x}_s$ , *i.e.* the time-differential of the PSS,  $x_s(t)$ . As discussed in the above references, the proper scale factor leads to  $u_1(t) = \dot{x}_s(t)$ .

The Kurokawa modelling approach [2], assumes a near-sinusoidal (N-SINUS) planar ( $n = 2$ ) PSS  $x_s(t) = \alpha + x_a(t) + \mathcal{O}(\epsilon)s(t)$  (see eq. (14) for description of terms). It then follows from the above discussion that  $u_1(t) = \dot{x}_s =$

$x_b(t) + \mathcal{O}(\epsilon)g(t)$  where  $x_b(t) = \dot{x}_a(t)$  is sinusoidal and  $g(t) = \dot{s}(t)$ . For the ILO configuration we are considering two modes  $\mu_1 = 0, \mu_2 < 0.0$  (see section 2.2). Due to the Floquet bi-orthogonality condition ( $v_i^\top(s)u_j(t) = \delta_{i,j}\delta(t-s)$ ) [5, 6], we get that  $v_1^\top(t)x_b(t) = 1$  and  $v_2^\top(t)x_b(t) = 0$ , for all  $t$ , to within an error of order  $|\epsilon| \ll 1$ . However, since  $x_b(t)$  is a sinusoidal planar (2D) solution this must imply that  $v_i(t)$ ,  $i = 1, 2$ , are both N-SINUS vector-functions. The standard formulation of the Kurokawa model [2, 3] does not involve modulated sources meaning that the noise matrix is constant,  $B \in \mathbb{R}^{2 \times p}$ , and  $\lambda_i(t) = v_i(t)^\top B$ ,  $i = 1, 2$ , are hence both zero-DC, N-SINUS  $p$ -dimensional vector-functions (see eqs. (4) and (5) and accompanying text).

From the above analysis,  $\lambda_1(t)$ , has zero DC, *i.e.*  $\Lambda_{1,0} = 0$ , which implies that the tensor/matrix expression in eqs. (9) and (10) reduce to

$$\Psi = \mathcal{O}(\epsilon) \quad (15)$$

$$\Phi_\rho = \frac{\sum_p U_{2,p} \Lambda_{2,\rho-p}^\top \Lambda_{2,\rho-1}^* U_{2,1}^\dagger}{j\omega_0(1-p) + 2|\mu_2|} + \mathcal{O}(\epsilon) \quad (16)$$

The Floquet mode vector,  $u_2(t) : \mathbb{R} \rightarrow \mathbb{R}^2$ , is zero-DC, N-SINUS (upto an error of  $|\epsilon| \ll 1$ ) which follows from  $v_2^\top(t)u_2(t) = 1$  and  $v_2$  being zero-DC, N-SINUS as discussed above. Hence,  $U_{2,p} = \mathcal{O}(\epsilon)$  for  $p \neq \pm 1$ . Hence, non-negligible terms (terms larger than  $\mathcal{O}(\epsilon)$ ) must correspond to indices  $p = \pm 1$  in eq. (16). However, since we must have  $|\mu_2| \ll \omega_0$  (holds for all relevant modes, see [17]) it follows that the terms corresponding to  $p = 1$  will dominate. Furthermore, from the above discussion we have  $\Lambda_{2,j} = \mathcal{O}(\epsilon)$ , for  $j \neq -1, 1$ . Combined this leaves us with the expression

$$\Phi_\rho = \frac{K_{-1}\delta_{\rho,0} + K_1\delta_{\rho,2}}{2|\mu_2|} + \mathcal{O}(\epsilon) \quad (17)$$

where

$$K_s = U_{2,1} \Lambda_{2,s}^\top \Lambda_{2,s}^* U_{2,1}^\dagger \quad (18)$$

Inserting eqs. (15), (17) and (18) into eqs. (6) to (8), and discarding all negligible terms of order  $\epsilon$ , the following expression for the PNOISE spectrum of the reduced-order K-ILO model is produced

$$\mathfrak{L}_{\text{ILO}}(\omega_m) \approx \frac{(\omega_0^2 c)^2}{(0.5\omega_0^2 c)^2 + \omega_m^2} + \frac{Z_{-1}}{|\mu_2|^2 + \omega_m^2} + \frac{Z_1 + (4\omega_0^2 c)}{(|\mu_2| + (2\omega_0^2 c))^2 + \omega_m^2} \quad (19)$$

where  $Z_s \in \mathbb{C}$  is a possibly complex scalar defined through

$$Z_s = [K_s]_{q,q} / \|X_{s,1}^{[q]}\|^2 \quad (20)$$

with  $q$  being the observation node (see discussion in sections 2.1 and 2.2 and eqs. (7) and (8)). The first term in eq. (19) represents the primary oscillator (see fig. 1.(b)) free-running PNOISE spectrum [4, 5] which we write  $\mathfrak{L}_P(\omega_m)$ . For most offsets of interest,  $\omega_m \gg 0.5\omega_0^2 c$ , as  $0.5\omega_0^2 c$  is a very small offset typically on the order of 1Hz or lower, The following approximation then holds [5]  $\mathfrak{L}_m(\omega_m) \approx (\omega_0^2 c)/\omega_m^2$  and using this expression we can carry out the following calculation

$$\mathfrak{L}_P(\omega_m)(\omega_m^2 + |\mu_2|^2) \approx (\omega_0^2 c/\omega_m^2)(\omega_m^2 + |\mu_2|^2) = \omega_0^2 c + (\omega_0^2 c/\omega_m^2)|\mu_2|^2 = \omega_0^2 c + \mathfrak{L}_P(\omega_m)|\mu_2|^2 \quad (21)$$

Finally, we want to show that  $|\mu_2| \gg 2\omega_0^2 c$  which means that the following relation

$$|\mu_2| \gg 2\omega_0^2 c \Leftrightarrow \frac{|\mu_2|}{\omega_0} \gg 4\pi \frac{c}{T_0} \Leftrightarrow -\frac{1}{2\pi} \ln(\iota_2) \gg 4\pi \frac{c}{T_0} \quad (22)$$

where  $T_0$  is the oscillation period ( $\omega_0 = 2\pi/T_0$ ) and we have introduced the Floquet characteristic multiplier,  $\iota_2 \in \mathbb{R}$ , through [4–6, 9]  $\iota_2 = \exp(-|\mu_2|T_0)$ . A reasonable estimate for normal operation would be  $\iota_2 \in (0.95, 0.7)$  since

$\iota_2 = 1.0$  corresponds to the uncoupled scenario (see [1]). So the minimal value in eq. (22) is taken for  $\iota_2 = 0.99$  (for this example). Using this estimate, eq. (22) gives

$$|\mu_2| \gg 2\omega_0^2 c \Leftrightarrow \frac{c}{T_0} \ll \ln(0.99)/(8\pi^2) \sim 10^{-4} \quad (23)$$

which generally will hold as  $c$  is a very small parameter. Of-course, as the value of  $\mu_2 \rightarrow 0$  (towards uncoupling) or the value of the phase-diffusion constant,  $c$ , increases (stronger P-OSC noise drive), this relation breaks down very fast. Since eq. (22) holds, at-least for reasonable values of  $\mu_2$  and  $c$ , we can approximate  $|\mu_2| + 2\omega_0^2 c \approx |\mu_2|$  in the denominator of the third term in eq. (18). Using this approximation together with the result in eq. (21) we can write eq. (19) as

$$\mathfrak{L}_{\text{ILO}}(\omega_m) \approx \mathfrak{L}_{\text{K-ILO}}(\omega_m) + \mathcal{O}(\epsilon) \quad (24)$$

where

$$\mathfrak{L}_{\text{K-ILO}}(\omega_m) = \frac{\mathfrak{L}_P(\omega_m)|\mu_2| + \Delta_0^{(K)}}{|\mu_2|^2 + \omega_m^2} \quad (25)$$

where  $\Delta_0^{(K)} \in \mathbb{R}$  is the real scalar

$$\Delta_0^{(K)} = Z_{-1} + Z_1 + 5(\omega_0^2 c) \quad (26)$$

which can also be written (see eq. (20))

$$\Delta_0^{(K)} = 2[U_{2,1} \Re\{\Lambda_{2,1}^\top \Lambda_{2,1}^*\} U_{2,1}^\dagger]_{q,q} / \|X_{s,1}^{[q]}\|^2 + 5\omega_0^2 c \quad (27)$$

## References

- [1] Djurhuus, Torsten, and Viktor Krozer. "A generalized model of coupled oscillator phase-noise response." *International journal of circuit theory and applications*, 50.1 (2022): 35-55.
- [2] Kurokawa, Kaneyuki. "Noise in synchronized oscillators." *IEEE Transactions on microwave theory and techniques*, 16.4 (1968): 234-240.
- [3] Ramirez, Franco, et al. "Phase-noise analysis of injection-locked oscillators and analog frequency dividers." *IEEE Transactions on Microwave Theory and Techniques*, 56.2 (2008): 393-407.
- [4] F. X. Kärtner, "Analysis of white and f- $\alpha$  noise in oscillators," *International Journal of Circuit Theory and Applications*, vol. 18, no. 5, pp. 485–519, 1990.
- [5] A. Demir, A. Mehrotra, and J. Roychowdhury, "Phase noise in oscillators: A unifying theory and numerical methods for characterization," *IEEE Transactions on Circuits and Systems I: Fundamental Theory and Applications*, vol. 47, no. 5, pp. 655–674, 2000.
- [6] T. Djurhuus, V. Krozer, J. Vidkjær, and T. K. Johansen, "Oscillator phase noise: A geometrical approach," *IEEE Transactions on Circuits and Systems I: Regular Papers*, vol. 56, no. 7, pp. 1373–1382, 2009.
- [7] B. Razavi, "A study of phase noise in cmos oscillators," *IEEE journal of Solid-State circuits*, vol. 31, no. 3, pp. 331–343, 1996.
- [8] C. Samori, A. L. Lacaita, F. Villa, and F. Zappa, "Spectrum folding and phase noise in lc tuned oscillators," *IEEE Transactions on Circuits and Systems II: Analog and Digital Signal Processing*, vol. 45, no. 7, pp. 781–790, 1998.
- [9] F. L. Traversa and F. Bonani, "Oscillator noise: A nonlinear perturbative theory including orbital fluctuations and phase-orbital correlation," *IEEE Transactions on Circuits and Systems I: Regular Papers*, vol. 58, no. 10, pp. 2485–2497, 2011.
- [10] T. Djurhuus, V. Krozer, J. Vidkjær, and T. K. Johansen, "Trade-off between phase-noise and signal quadrature in unilaterally coupled oscillators," in *IEEE MTT-S International Microwave Symposium Digest, 2005*. IEEE, 2005, pp. 4–pp.

- [11] T. Djurhuus, V. Krozer, J. Vidkjær, and T. K. Johansen, "Nonlinear analysis of a cross-coupled quadrature harmonic oscillator," *IEEE Transactions on Circuits and Systems I: Regular Papers*, vol. 52, no. 11, pp. 2276–2285, 2005.
- [12] —, "Am to pm noise conversion in a cross-coupled quadrature harmonic oscillator," *International Journal of RF and Microwave Computer-Aided Engineering*, vol. 16, no. 1, pp. 34–41, 2006.
- [13] T. Djurhuus and V. Krozer, "A study of amplitude-to-phase noise conversion in planar oscillators," *International Journal of Circuit Theory and Applications*, vol. 49, no. 1, pp. 1–17, 2021.
- [14] Chang, Heng-Chia, et al. "Phase noise in coupled oscillators: Theory and experiment." *IEEE Transactions on Microwave Theory and Techniques* 45.5 (1997): 604-615.
- [15] Chang, Heng-Chia, et al. "Phase noise in externally injection-locked oscillator arrays." *IEEE Transactions on Microwave Theory and Techniques* 45.11 (1997): 2035-2042.
- [16] Lynch, Jonathan J., and Robert A. York. "Synchronization of oscillators coupled through narrow-band networks." *IEEE Transactions on Microwave Theory and Techniques* 49.2 (2001): 237-249.
- [17] Maffezzoni, Paolo, Federico Pepe, and Andrea Bonfanti. "A unified method for the analysis of phase and amplitude noise in electrical oscillators." *IEEE transactions on microwave theory and techniques* 61.9 (2013): 3277-3284.